

MATERIALS AND COMPONENTS DEVELOPMENT FOR ADVANCED TURBINE SYSTEMS - ODS ALLOY DEVELOPMENT

B. S.-J. Kang¹, K. Ogawa², L. Ma³, , M. A. Alvin⁴, N. Wu¹, and G. Smith⁵

¹Mechanical and Aerospace Engineering Department, West Virginia University

²Fracture and Reliability Research Institute, Tohoku University, Japan

³Harry Reid Center for Environmental Studies, University of Nevada

⁴US DOE National Energy Technology Laboratory

⁵Special Metals Inc.

ABSTRACT

Oxide dispersion strengthened (ODS) alloys have been under intensive development over the past four decades due to their excellent high-temperature creep strength and good oxidation resistance. Nickel-based ODS alloys are the combination of gamma prime (γ') strengthened superalloy with yttrium oxide evenly distributed throughout the matrix to allow the strength to be maintained to much higher temperatures than conventional superalloys. ODS alloys are being considered for high temperature applications in advanced power plant such as heat exchanger tube, boiler, superheating tube, vane or turbine blade. However, a key factor that limits their wide usage is the high manufacturing cost. In this research, a powder mixing technique, Hosokawa mechano chemical bonding (MCB) technology, is used to produce ODS powder mixtures with the aims of obtaining comparable or enhanced ODS powders with much less manufacturing cost. One of the key ideas of the proposed Hosokawa method is the use of nano-sized oxide particles, which, through the processing, will grow on the surfaces of larger micron-sized master particles and make homogeneous dispersions. In this paper, preliminary results are shown and discussed. Four batches of alloying powder samples, based on composition of Ni-20Cr-5Al-1.5 Y₂O₃ and Ni-20Cr-5Al-3W-1.5 Y₂O₃ (wt%) and different sizes of master alloy powders (Ni and Cr), have been prepared by the MCB process. The starting powders and MCB-processed powders were subjected to microscopic and spectroscopic characterization using X-ray diffraction (XRD), scanning electron microscopy (SEM), and transmission electron microscopy (TEM) to examine the microstructure, morphology and mixing homogenization of alloying powders processed by MCB. The results show that during the MCB processes, the particles in alloying powders were subjected to high speed colliding, cold weld and plastic deformation, forming the composite particles hosted by Ni or Cr master elemental powders. A thin film containing the alloyed elements such as Al, Y, O and W was observed to distribute throughout the composite particles. Lowering the size of master powders would improve the homogenization of alloying powder mixture, building up a smooth thin film coated around the composite particles. In addition, the MCB process in this study could manifest the crystalline nano-sized Y₂O₃ particles as the amorphous film bonded with the host composite particles, resulting in the disappearance of Y₂O₃ peak in the XRD spectrum. When fabricated with additional high energy ball milling, the resulting alloys are expected to have enhanced mechanical properties for use in advanced turbine applications.

ODS alloys are used not only in the form of bulk components but also in the form of coatings. In this research, we attempt to combine the Hosokawa MCB-processed ODS powders with high pressure cold spray coating technique for ODS coatings. This new ODS coating development will be able to deposit high-quality ODS coatings on various solid substrates. In this paper, using the MCB-processed ODS powders and cold spray method, preliminary results of ODS coatings on Inconel 625 are demonstrated, which shows thick ODS coating is possible with high deposition efficiency. Very good interface (coating/substrate) adherence is also observed.

INTRODUCTION

Nickel-based oxide dispersion-strengthened (ODS) superalloys such as MA 957 or MA 6000 produced through the mechanical alloying (MA) and consolidation process exhibit the intermediate temperature strength as well as elevated temperature strength and creep resistance by means of the combined strengthening of gamma prime precipitates and nano-sized yttrium oxide particles [1-3]. The ODS Ni-based superalloys are very promising for use in aircraft and advanced gas turbine engines. Also since yttrium oxide particles serve for interfacial pinning of the moving dislocations, ODS alloys offer not only the improved creep resistance at elevated temperatures (up to 1200°C) but also low void swelling at condition of high energy high speed neutron irradiation. For example, ODS strengthened ferritic-martensitic (F/M) Fe-Ni-based alloys such as PM 2000 and MA 956 have been selected as the potential materials used as low irradiation swelling material for the future generation of high temperature gas cooled nuclear reactors and fusion applications such as generation IV nuclear fission [4,5]. Fabrication of ODS alloys is a complicated, costly and time-consuming process, which involves a mechanical alloying (MA) powder metallurgical process, consolidation by hot deformation and post heat treatment process [6,7]. During MA process, the elemental alloy powders or oxide compounds are subjected to the high energy ball milling or rod milling for anywhere between 24 to 72 hours to produce homogeneously mixed, heavily deformed, cold welded composite particles. The nano-sized yttrium oxide particles are expected to form the dispersion throughout the master particles. After MA processing, the mixed and alloyed powders are then canned and consolidated by hot isostatic pressing (HIP) or hot extrusion. After consolidation, the material is then hot worked to semifinishes. The hot worked material is followed by annealing and aging to yield the recrystallized microstructure including the coarse and highly elongated grain structure and strengthening precipitates. The complicated fabrication process has become a major barrier to commercially produce the ODS strengthening materials with competitive cost as compared to single crystal alloys. The first step of the ODS alloy processing technology is the MA process, during which the metal powders and hard oxide particle are ball milled or rod milled in dry, inert atmospheres up to 72 hours to form a fine and homogeneous dispersion of the oxide particles around the master alloyed powders [7]. In this study, a Mechano Chemical Bonding (MCB) technique was employed to execute the first stage of the mechanical alloying (MA) process and prepare the ODS alloyed powders instead of the conventional ball milling or rod milling technique. In this paper,

we present preliminary results of the MCB-processed ODS powders. Alloying powders, based on Ni-20Cr-5Al and Ni-20Cr-5Al-3W (wt%) with different sizes of master alloy powders (Ni and Cr) and nano-sized yttrium oxide (Y_2O_3), were subjected to mechanical compression, shear and impact forces using a high energy MCB system for only 30 minutes. The starting and as-initially-blended elemental powders as well as MCB-processed powders were examined and analyzed microscopically and spectroscopically using TEM, SEM and XRD to identify the mechanical alloying effects such as powder microstructure, morphology, and mixture homogeneity. As a preliminary research phase, the goal of this study is to examine the mechanical alloying effects produced by the proposed MCB technique. The end products, MCB-processed ODS alloyed powders, will be either used as spray powders for advanced coating or followed by conventional ball milling (with reduced milling time), canning, HIP, hot rolling and annealing to form final ODS products in the next research phase. This study is an attempt to fabricate the ODS alloyed powders using the proposed MCB technique as a substitute or to simplify the MA process.

MATERIALS AND EXPERIMENTS

Materials

As shown in Table 1, commercial metal and ceramics powders including Y_2O_3 (< 50 nm, 99.99% pure), Al (4.5-7 μm , 97.5% pure) and Ni (4~8 μm , 99.9% pure) were purchased from Sigma Aldrich Inc., Alfa Aesar and Atlantic Equipment Engineers respectively. Cr (7.5~10 μm and 8~12 μm , 99.5% pure), W (0.5~1 μm and 2~4 μm , 99.95% pure,) and High Density Ni powder (8~15 μm) were provided by F.W. Winter Inc. & Co., Buffalo Tungsten Inc., and Inco Special Products respectively. These powders were stored separately in an inert environment in sealed bottles full of argon gas. Four batches of ODS alloying powder samples were prepared according to master alloy powder size (Ni and Cr) with an addition of trace refractory powder, tungsten powder, to explore the effects of master powder size and trace refractory powder on mechanical alloying produced by the MCB process. Considering the short time milling as well as no ball-powder-ball collision involved during MCB process in this study, the average sizes of all starting powder constituents ranged from 0.5 to 15 microns. For conventional ball milling or rod milling MA process, however, the starting powders usually have average diameters ranging from 1 to 500 micron [7]. Since aluminum powder is usually soft and easy to deform, the size of aluminum powder was kept constant. In order to examine the dispersion effect caused by MCB-induced mechanical alloying, the composition and particle size of yttrium oxide nanoparticle were kept constant in all powder samples. Early studies showed that the addition of hard-to-deform refractory elements, such as Mo, Ta, or W, to ODS alloys could stabilize the yttrium oxide particles in ODS alloys at elevated temperatures [8]. In this study, different sizes of tungsten particles were selected to blend with the powders for examining their effects on MCB process and further properties of final ODS products in the next phase. For each ODS powder sample, the powder components were weighted according to the designed composition, initially mechanically blended, and then placed into a bottle that was sealed and filled with argon gas to prevent oxidation of powders. All these operations were done under argon gas

environment inside a glove box chamber. Each bottle containing ODS powder sample weighed approximately 200g. Table I lists the sample identification number, element composition (wt%), and powder sizes.

Mechanical Alloying by MCB Process

The as-initially-blended powder samples were stored in bottles filled with argon gas and sent to Hosokawa Micron Powder Systems, Summit, NJ, for the preparation of ODS powders using MCB technique. The MCB Technology was developed by Hosokawa Micron Corporation, Osaka, Japan and has been utilized to make various composite particles used in the fields of functional gradient materials, batteries, cermets, fuel cells, polymers, cosmetics, and pharmaceuticals. It is often considered as an enhancement or alternative to the conventional mechanical alloying (MA) process using balling milling or rod milling [9-10]. Also, the newly developed MCB processing technique is simple, environmentally friendly, and can be scaled up to 300 liters per batch. The MCB particle bonding process takes place in the solid state without needing solvents or external heating. During MCB processing in this study, the starting powder mixtures were subjected to high compression, shear, and impact forces as they pass through a narrow gap in a high speed rotating device (typically around 4000 rpm). As a result, the particles were dispersed, mixed, shaped, and bonded together. Consequently, the composite particles consisting of various combinations of the starting ingredients were formed. In this study, the starting powder mixtures were MCB processed for only 30 minutes. It was expected to have Y_2O_3 nanoparticles dispersed and bonded onto the surfaces of larger hosting particles such as Ni and Cr particles, which in turn creating oxide dispersion effects. After MCB processing, the powders were stored in the sealed bottles filled with argon gas. Small amount of MCB-processed (5 g) powders were taken for analysis using transmission electron microscopy (TEM), scanning electron microscopy (SEM) and X-ray diffraction (XRD).

RESULTS AND DISCUSSIONS

Starting Materials Characterization

Two representative starting powders, as-received nano-sized Y_2O_3 powder and mixture of starting powder sample A2 (as-blended) that contains all starting ingredients, were selected to examine the morphology and crystallinity before MCB process. The as-received Y_2O_3 particles were white in color and Ni, Cr, Al and W particles were gray in color. Figure 1 presents the typical XRD patterns of the as-blended powder sample A2 and as-received Y_2O_3 powder. The XRD pattern of sample A2 showed well-defined sharp diffraction peaks, which were identified as reflection of Al, Cr, Ni and W. The diffraction peak of nano-sized Y_2O_3 in XRD spectrum was observed with low intensity and broadened width, indicating that Y_2O_3 particles in as-blended sample powder A2 are crystalline and have minor fraction and fine particle size. The XRD pattern of pure Y_2O_3 powder showed the broadened multiple diffraction peaks with strong intensity, confirming the crystallinity and fine size of the as-received Y_2O_3 powders. Figure 2

exhibits TEM micrographs of as-received Y_2O_3 particles and as-blended A2 sample, showing that the as-received nano-sized Y_2O_3 particles are highly agglomerated even after being ultrasonically agitated for 5 minutes, as seen in Figure 2(a). The size of Y_2O_3 particles was not uniform ranging from 10 to 45 nm. Presumably, the surface tension of the nano-sized particles was related to the agglomeration of Y_2O_3 powders in TEM imaging. For as-blended powder sample A2, the agglomeration of nano-sized Y_2O_3 particles was observed as well. In addition, Y_2O_3 particles tended to attach on the surface of larger particles as shown in Figure 2(b) also caused by the surface tension. The hosting particles, Cr and Ni particles, in sample A2 with average size of 7.5-10 and 4-8 μm respectively were too big for electron transmission, resulting in the dark contrast in the TEM imaging.

Characterization of MCB-processed Powders

Figure 3 presented the XRD patterns of as-received Y_2O_3 powder, as-blended A2 powders, and MCB-processed sample A2. As shown in Figure 3, the diffraction peaks of all alloying elements, Al, Cr, Ni and W, were observed in XRD spectrum. All diffraction peaks had identical width in spectrum, suggesting there is no significant change in size of elemental powders after MCB process. However, the peak of Y_2O_3 is not present in the MCB-processed sample A2, suggesting the MCB process would change the crystallographic structure of the nano-sized Y_2O_3 particle. Comparing to the starting as-blended powder samples, all the MCB-processed powder samples showed the diffraction peaks with similar width at same diffraction angles, 2θ , as well as absence of new detectable peaks, indicating that these end products processed by MCB are still intact mixture of starting ingredients without any undesirable reactions occurring among the elemental powders. XRD analysis of all samples including starting and end materials indicates that the MCB process in this study would not change the crystallographic structure and particle size of process elemental powders, Al, Cr, Ni and W, but change the crystallographic structure of nano-sized Y_2O_3 particle, resulting in the disappearance of Y_2O_3 peak in XRD spectrum.

SEM analysis was conducted on the MCB-processed powder samples, A1 and A2, with smaller master powder size than samples, B1 and B2. SEM micrographs in Figure 4 and Figure 5 showed the morphology, topology, and size of the MCB processed powder sample A1 and A2. After MCB processing, the master elemental particles identified as Ni and Cr by EDX in powder sample A1 and A2 kept spherical, minor particles identified as mostly Al by EDX were formed the fragments with random shape and size as seen in Figure 4(a) and Figure 5(a). The minor particles such as Al and W tended to attach on the surface of the large particles to form the composite particles. Close views of sample A1 and A2 as shown in Figure 4(b) and Figure 5(b) exhibited the smooth surface embedded with small particles, suggesting the particles were subjected to deformation on each other and the small sized particles such as Al and W were embedded into the matrix of large particle forming the composite particles. There were still a few of small particles, which have not fully embedded into matrix forming the rough surface in the mixture of powders. SEM EDX line scanning and elementary mapping mode were utilized to examine the elemental distribution of the MCB processed powder samples, A1 and A2,

as shown in Figures 6 and 7. As EDX mapping micrographs exhibited in Figures 6(a) and 7(a), the master elemental powders such as Ni and Cr particles played the roles as hosting particles to entrap the minor elemental powders such as Y_2O_3 , Al and W particles. Mapping micrographs evidently showed that Y_2O_3 and W have been dispersed homogeneously throughout the host particles after MCB processing. Smaller-size deformed aluminum fragments were found attached on the hosting particles or separately distributed in mixture of powders. The distribution of aluminum fragments appeared heterogeneous among the powders, suggesting that the soft aluminum particles were subjected to mechanical deformation and fracturing, forming fragments with reduced size during MCB processing. The aluminum fragments were randomly distributed or bonded on the hosting particles. The inter-diffusion of Y_2O_3 , Al and W on hosting particles was observed in the mapping micrographs. SEM EDX line scanning examination was conducted across several particles along the arrow-marked direction as indicated in Figures 6(b) and 7(b). The results as presented in Figures 6(b) and 7(b) showed that the presence of element Y, O and W was detected throughout the hosting particles, indicating MCB process allowed these elements to be dispersed and bonded with the hosting particles. The SEM EDX line scanning also confirmed the heterogeneous distribution of aluminum. SEM microscopic and spectroscopic characterization of sample A1 and A2 summarized that elemental powder Y_2O_3 and W in sample A1 and A2 had been mixed homogeneously and the composite particles hosted by the master elemental particles such as Ni and Cr could be created through the MCB processing. The composite particles contained elements of Y, O and W, which had been dispersed and mixed with hosting particles through MCB processing. The soft aluminum powders were deformed and fractured to form fragments and attached on the hosting particles or became discrete particles after MCB processing.

The presence of elements Y and O confirmed by EDX mapping and line scanning in SEM imaging showed the discrepancy with the results of XRD, wherein the Y_2O_3 peak was not detected. To explore the reason for absence of Y_2O_3 peak in XRD pattern of A1 and A2 sample as well as identify the microstructure of composite particle induced by MCB processing, sample A1 and A2 were subjected to TEM and HRTEM analysis. Figures 8 and 9 presented the TEM and HRTEM micrographs of sample A1 and A2. The low magnification of TEM BF images of sample A1 and A2 as seen in Figures 8(a) and 9(a) showed that the hosting particles displayed dark contrast due to their thickness and the detailed information was invisible. Increasing the magnification of TEM imaging allowed a thin film with thickness of 20-25 nm around the hosting particles to be observed in sample A1 and A2. HRTEM images of the thin films in sample A1 and A2, as shown in Figures 8(b) and 9(b), showed the thin film was amorphous and very few crystalline structures was exposed, as suggested by the embedded FFT images showing diffusive feature and spots associated with amorphous and crystalline structure respectively. Also, the thin film around the hosting particle was observed in Z-contrast image of sample A1, generated in STEM mode, as shown in the inset image of Figure 10, wherein the thin film showed the bright contrast around the particle. As expected, EDX examination of these thin film regions confirmed that the thin film contained elements of Ni, Al, Y and O as seen in Figure 10, wherein the convergent electron beam with a probe size of 0.2 nm was located in the particle edge as marked in figure to examine the

chemical composition of the dedicated location. Therefore, based on the SEM, TEM, HRTEM, STEM and STEM/EDX analysis, it could be concluded that Y_2O_3 was manifested as the amorphous thin film dispersed and coated on the hosting particles after MCB processing, resulting in disappearance of Y_2O_3 peak in XRD spectrum. The tiny fraction of Y_2O_3 crystalline particles might still exist within the film which was too weak to be detected by XRD.

Early studies indicated that the particle size of powders usually affected the morphology and mixing homogeneity of ODS alloy powders from the mechanical alloying [7, 11]. Figure 11 showed the SEM micrographs of powder sample B1 and B2, wherein the hosting powders such as Ni and Cr have bigger size, 7-12 and 8-12 μm respectively, than sample A1 and A2. Unlike sample A1 and A2 that included the composite particles with milled smooth surface and spheroid, SEM images of powder sample B1 and B2 showed that lots of composite particles had been built up and the surface of particle was relatively rough with the attachment of many small fragments. The SEM images also showed that many voids, small particles and un-deformed particles on the composite surface. It suggested that the cold-welding of fragments had not been fully completed to form the elemental inter-diffused composite particles with smooth surfaces and the powder mixture appeared to be heterogeneous. Similarly, as displayed in Figures 12 and 13, SEM EDX mapping images and EDX line scanning curves of sample B1 and B2 showed that hard tiny particles such as W and Y_2O_3 could be dispersed throughout the hosting Cr or Ni particles during MCB processing. The Al particles could be deformed, fractured and attached on the hosting particles or stayed as discrete particles.

The thin films with thickness of 40-50 nm around the hosting particles were also observed in the TEM BF images of sample B1 and B2, as seen in Figures 14 and 15. HRTEM images of the thin film confirmed that most regions of thin film in B1 and B2 are amorphous. Also, this result explained the absence of Y_2O_3 peak in XRD spectrum of sample B1 and B2. Lots of inclusions were found within the thin film and HRETM confirmed the crystalline characteristic of inclusions as seen in FFT image of Figure 14(b). For sample B2, the full nano-sized crystalline particle was found as shown in Figure 15(b) and was identified as the Y_2O_3 by examination of particle size and d-spacing. The presence of inclusions within thin film of sample B1 and B2 suggested that increasing the particle size of hosting powder would cause the heterogeneity of powder mixtures during MCB processing. To get better MA effects using MCB process, a proper combination of the particle sizes of hosting and elemental powders, energy input, and MCB processing time should be optimized.

ODS Coating by Cold Spray

Cold-gas dynamic-spray process, which is often referred as Cold Spray was originally developed in the mid-1980s by Russian scientists at the Institute for Theoretical and Applied Mechanics of the Siberian Division of the Russian Academy of Science in Novosibirsk [12] and has become an emerging coating technology with extensive R&D effort around the globe since mid 1990s. However, to this date, cold spray is still considered as a relatively new coating technique and considerable R&D efforts are

needed to both understand and control the coating process to achieve the desirable coatings [13]. Figure 16 shows a typical cold spray schematic setup in which a particle-laden (typically 1–50 μm in diameter) gas jet impinges on a solid surface at a high velocity (ranging from 300 to 1200 m/sec or subsonic to supersonic) and a temperature that is much lower than the melting point of the starting powder [12-14]. In cold spray deposition, microstructure of the coated layer experiences little changes, and little or no oxidation, decomposition, or phase transformation. Most metals such as Cu, Cr, Al, Ni, Ti and Ni-based alloy can be deposited by cold spray [12-16]. Also, cermets [18] and ceramics [19] can be coated into a substrate to form a thin coating layer using cold spray technology. Comparing to other thermal spray methods, cold spray costs less and is capable of thick deposition with higher deposition efficiency.

To the best of our knowledge, ODS coating has not been applied before using the cold spray technology. In this research, the MCB-processed ODS powder samples (A1, A2, B1 and B2) were coated on Inconel 625 substrate using low pressure (LP) cold spray. Figure 17 shows the LP cold spray system (DymetTM) used in this study. Figure 18 shows the as-sprayed ODS coatings with the following processing conditions: 400 °C gas heating, 0.8 MPa Air (or 300 m/sec velocity), 10 mm off the target, manual operation with four passes. Figures 19 and 20 show optical micrographs of the cross section and coating/substrate interface. As shown, relative thick coatings (Figure 19) and excellent adhesion (Figure 20) are noted. Figures 21 and 22 show A1 and A2 coatings with associated EDX analyses. As shown, in both cases, the coatings are dense and well-adherent to each other, i.e. relative uniform. Most Al and Cr particles are fully deformed and yttrium oxides are distributed uniformly. Most nickel particles keep their spherical shape with partial deformation only. Figures 23 and 24 show B1 and B2 coatings with associated EDX analyses. As shown, in both cases, similar to the A1 and A2 coatings, the coatings are well-adherent to each other with good coating/substrate interfacial adherence and yttrium oxides are also distributed uniformly. However, pores are present sporadically, this may be due to the relatively large, non-deformed Ni splats. These preliminary results indicate ODS coating using cold spray technique is possible.

FUTURE RESEARCH

In this paper, we present our first-year research effort. More studies on the MCB-processed ODS powders are on-going. Research effort will be focused on combining the MCB process with the follow-up ball-milling to fabricate ODS powders with reduced manufacturing cost and improved ODS properties. Also, concerted effort will be on more trial runs of ODS coatings using high pressure (HP) cold spray. Post heat treatment and annealing on the ODS coatings are planned in second-year research. A custom-made heat treatment chamber apparatus is under construction with a water-cooled specimen-holding stage inside the chamber. The apparatus has the capability to conduct isothermal or cyclic thermal heat treatment as well as annealing on the ODS coating layer (up to 1380 °C and in inert gas environment) while the substrate is protected by the water-cooled stage. Future research activities include performance characterization of the corrosion and mechanical property performance of the ODS coatings under simulated turbine conditions.

CONCLUSIONS

A Mechano Chemical Bonding (MCB) technique was used to homogenize nano-sized oxide in ODS powders. Four batches of alloying powder samples were prepared by the MCB process and characterized using SEM, TEM, HRTEM and XRD. The results suggested that: (1) the MCB processing enabled the hosting particles such as Ni and Cr particles to be coated with a nano-sized thin film containing elemental particles of W and Y_2O_3 , (2) during MCB processing, the soft aluminum particles were subjected to deformation and fragmentation and randomly bonded onto the hosting particles or existed as discrete particles in the mixture, (3) small particle size of hosting powders such as Cr and Ni would improve the homogeneity of alloying powder mixture and help building up a smooth thin film around the hosting particles, (4) MCB process could transform crystalline nano-sized Y_2O_3 particles to an amorphous thin film bonded on the surfaces of host particles, causing the disappearance of Y_2O_3 peak in the XRD spectrum, (5) with increasing processing time, the MCB process can potentially be an effective method to fabricate the ODS alloying powders instead of the conventional mechanical alloying process using ball or rod milling, and (6) further studies on the effects of MCB processing condition and time on microstructure and morphology of ODS alloying powders are necessary to optimize the process.

We also demonstrated ODS coatings on superalloy substrate using LP cold spray technique. Thick and relatively uniform coating is possible with high deposition efficiency and good interfacial coating/substrate adherence.

ACKNOWLEDGEMENT

This research is supported by US Department of Energy, National Energy Technology Laboratory, Advanced Research Materials (ARM) Program under RDS Contract DE-AC26-04NT41817.606.01.01. The encouragement and support by Patricia Rawls and Robert Romanosky, Program Managers, for this exploratory research is very much appreciated.

REFERENCES

1. T.E. Howson, D.A. Mervyn, and J.K. Tien, "Creep and Stress Rupture of a Mechanically Alloyed Oxide Dispersion and Precipitation Strengthened Nickel-Base Superalloy," *Met. Trans. A*, vol. 11A, pp. 1609-1616, (1980).
2. T.S. Chou and H.K.D.H. Bhadeshia, "Crystallographic Texture in Mechanically Alloyed Oxide Dispersion-Strengthened MA956 and MA957 Steels," *Met. Trans. A*, vol. 24A, pp. 773-779, (1993).
3. M. Haghi and L. Anand, "High Temperature Deformation Mechanisms and Constitutive Equations for the Oxide Dispersion-Strengthened Superalloy MA 956," *Met. Trans. A*, vol. 21A, pp. 353-364, (1990).

4. Shigeharu Ukai, Masayuki Fujiwara, "Perspective of ODS Alloys Application in Nuclear Environments," *J. Nucl. Mater.* 307–311, pp 749–757, (2002).
5. R. Schaublin, A. Ramar, N. Baluc, V. de Castro, M.A. Monge, T. Leguey, N. Schmid, C. Bonjour, "Microstructural Development under Irradiation in European ODS Ferritic/martensitic Steels," *J. Nucl. Mater.* 351, pp. 247–260, (2006).
6. C. Suryanarayana, "Recent Developments in Mechanical Alloying," *Rev. Adv. Mater. Sci.* 18, pp. 203-211, (2008).
7. P. S. Gilman, and J. S. Benjamin, "Mechanical Alloying," *Ann. Rev. Mater. Sci.* 13, pp 279-300, (1983).
8. M.S.A. Karunaratne, C.M.F. Rae, and R.C. Reed, "On the Microstructural Instability of an Experimental Nickel-Based Single-Crystal Superalloy," *Met. Trans. A*, vol. 32A, pp. 2409-2421, (2001).
9. Nicholas J. Welham, Paul E. Willis, and Tony Kerr, "Mechanochemical Formation of Metal–Ceramic Composites," *J. Am. Ceram. Soc.*, 83 [1], pp33-40, (2000).
10. J.G. Nam and J.S. Lee, "Mechano-Chemical Synthesis Of Nanosized Stainless Steel Powder," *Nano Structured Materials*, Vol. 12, pp. 475-478, (1999).
11. M. Bodart, R. Baccino and E. Moret, "Elaboration and Study of Mechanically Alloyed ODS Ferritic Stainless Steel," *J. De Physiquiv IV, Colloque C7, supplement au J. de Physique III, Volume 3, November*, pp. 709-714, (1993).
12. A.P. Alkhimov, A.N. Papyrin, V.F. Dosarev, N.I. Nestorovich, M.M. Shuspanov, Gas Dynamic Spraying Method for Applying a Coating, US Patent 5,302,414, 12, April (1994).
13. J. Karthikeyan, "Cold Spray Technology: International Status And USA Efforts," ASB Industries Inc, December 2004 (available in web site: www.asbindustries.com).
14. R.B. Bhagat, M.F. Amateau, A.N. Papyrin, J.C. Conway Jr., B. Stutzman Jr., B. Jones, Thermal Spray: A United Forum for Scientific and Technological Advances, ASM International, C.C. Berndt (Ed.), Materials Park, OH, pp.361–367, (1997).
15. T. Stoltenhoff, H. Kreye, H.J. Richter, H. Assadi, Thermal Spray 2001: New Surfaces for a New Millennium, ASM International, C.C. Berndt, K.A. Khor, E.F. Lugscheider (Eds.), Materials Park, OH, pp.409–416, (2001).
16. M. Grujicic, C.L. Zhao, C. Tong, W.S. DeRosset, D. Helfrich, "Analysis of the Impact Velocity of Powder Particles in the Cold-gas Dynamic-spray Process," *Materials Science and Engineering A368*, pp. 222–230, (2004).
17. R. Maev, E. Strumban, L. Leshchynsky and M. Benetau, "Supersonically Induced Mechanical Alloy Technology (SIMAT) and Coatings for Automotive and Aerospace Applications," *Cold Spray 2004: An Emerging Spray Coating Technology*, ASM International, Akron, OH, September 27-28, (2004).
18. J. Karthikeyan, C.M. Kay, J. Lindemann, R.S. Lima, C.C. Berndt, Thermal Spray 2001: New Surfaces for a New Millennium, C.C. Berndt, K.A. Khor, E.F. Lugscheider (Eds.), ASM International, OH, pp.383–387, (2001).
19. G.-J. Yang, F. Han, C.-J. Li, in: X. Huang (Ed.), *Proceedings of the Fifth International Seminar and the Sixth China National Thermal Spraying Conference*, Anshan, China, pp.56–61, May 21–25, (2002). (in Chinese).

Table 1 ODS Sample Powder ID, Composition, and Particle Size

	Cr (7.5~10 μm)	Al (4.5 ~ 7 μm)	Y ₂ O ₃ < 50nm	W (~1 μm)	Ni (4 ~ 8 μm)
A1	20	5	1.5	0	73.5
A2	20	5	1.5	3	70.5
	Cr (8~12 μm)	Al (4.5 ~ 7 μm)	Y ₂ O ₃ < 50nm	W (2~4 μm)	Ni (8~15 μm)
B1	20	5	1.5	0	73.5
B2	20	5	1.5 </td <td>3</td> <td>70.5</td>	3	70.5

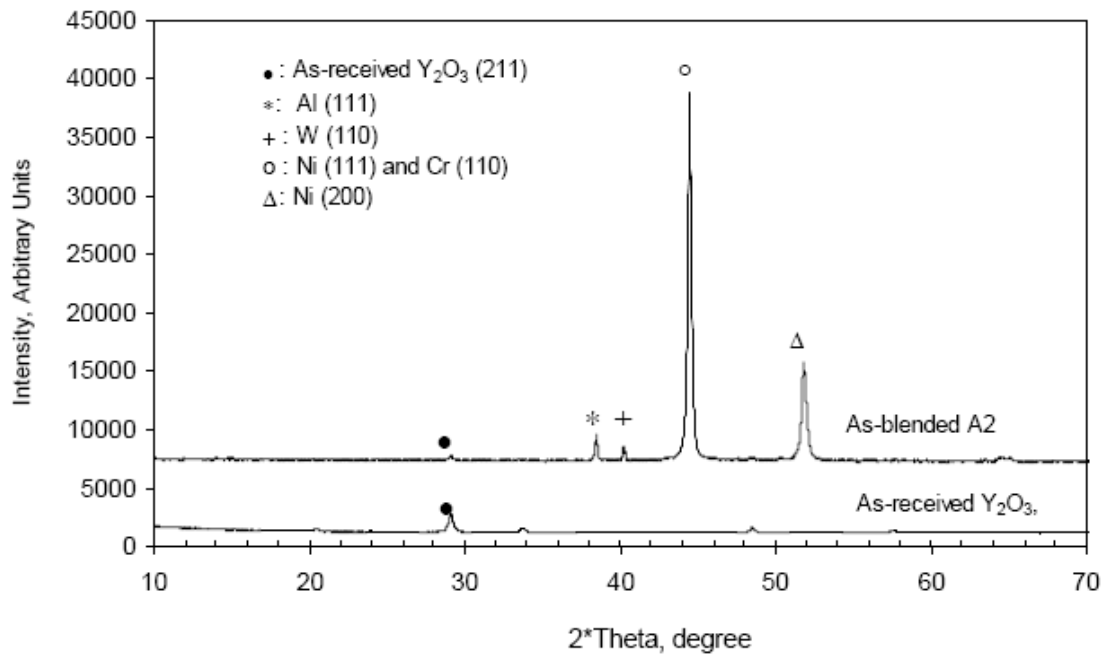


Figure 1 XRD patterns of starting powders

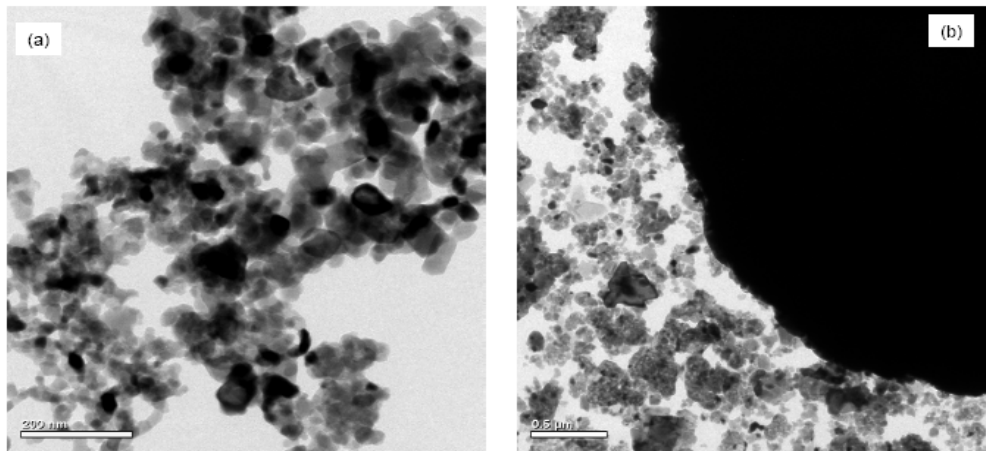


Figure 2 TEM micrographs of starting powders
 (a). As-received Y_2O_3 particle; (b) As-blended sample powder A2

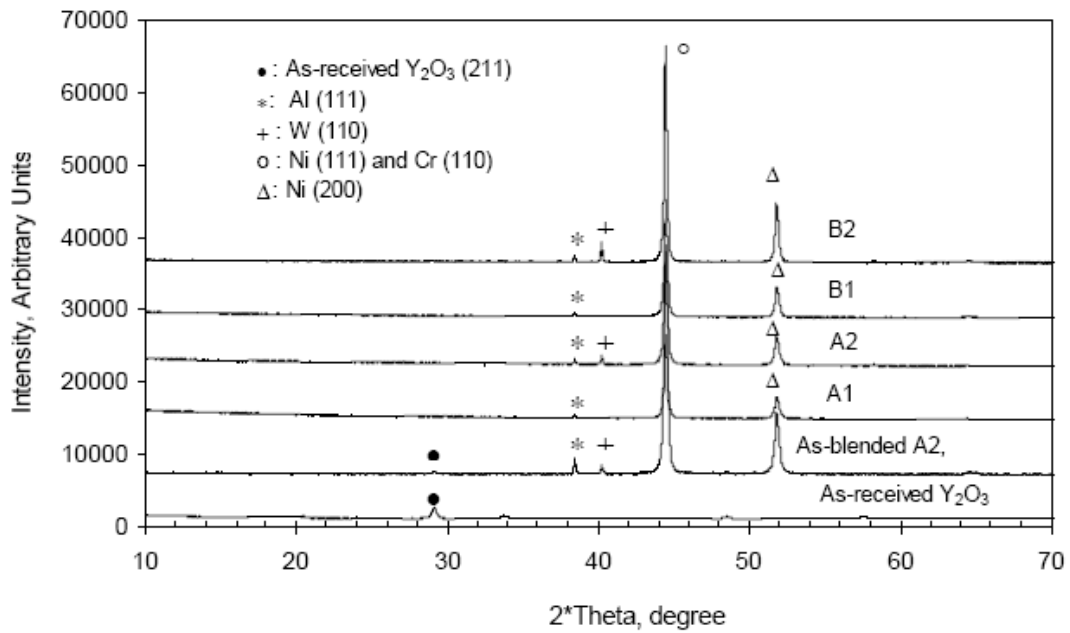


Figure 3 XRD patterns of starting and MCB processed powders

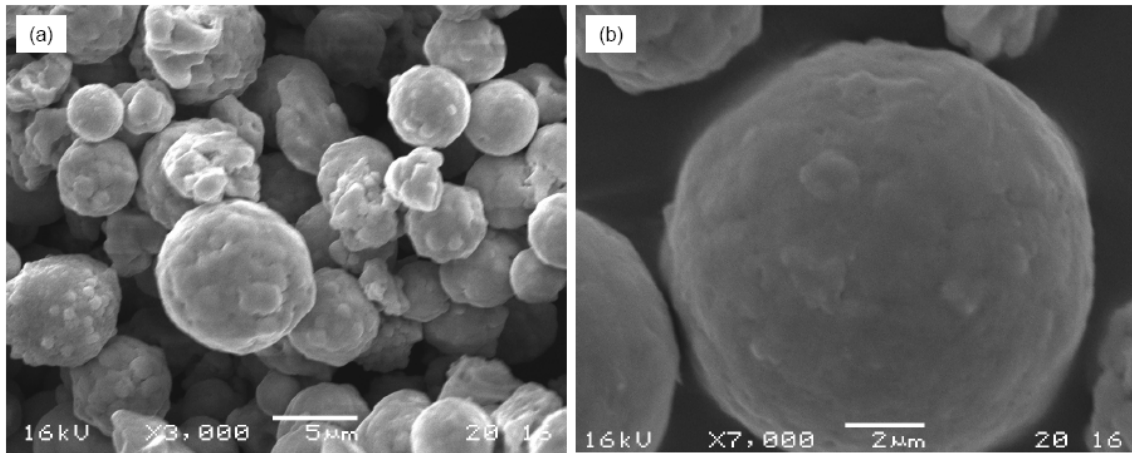


Figure 4 SEM micrographs of MCB processed powder sample A1
(a). Low magnification of sample A1; (b) close view of (a)

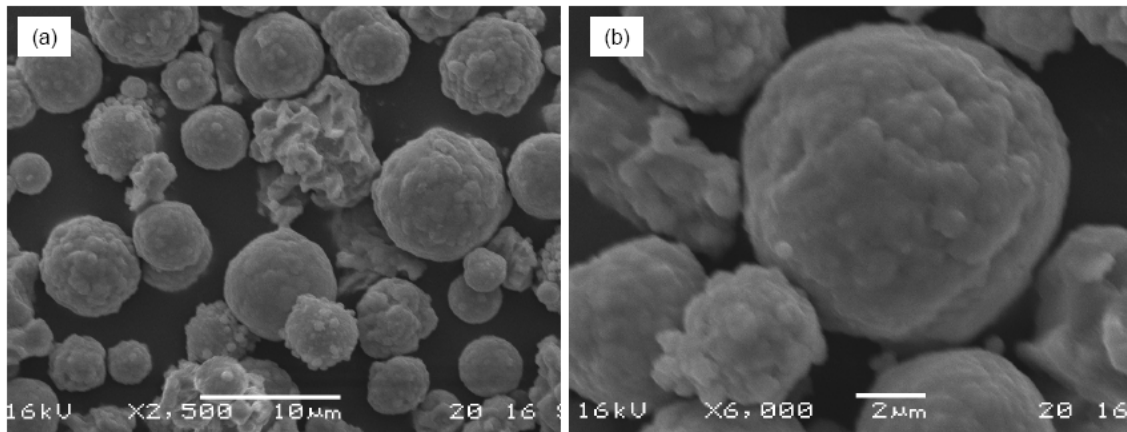


Figure 5 SEM micrographs of MCB processed powder sample A2
(a). Low magnification of sample A2; (b) close view of (a)

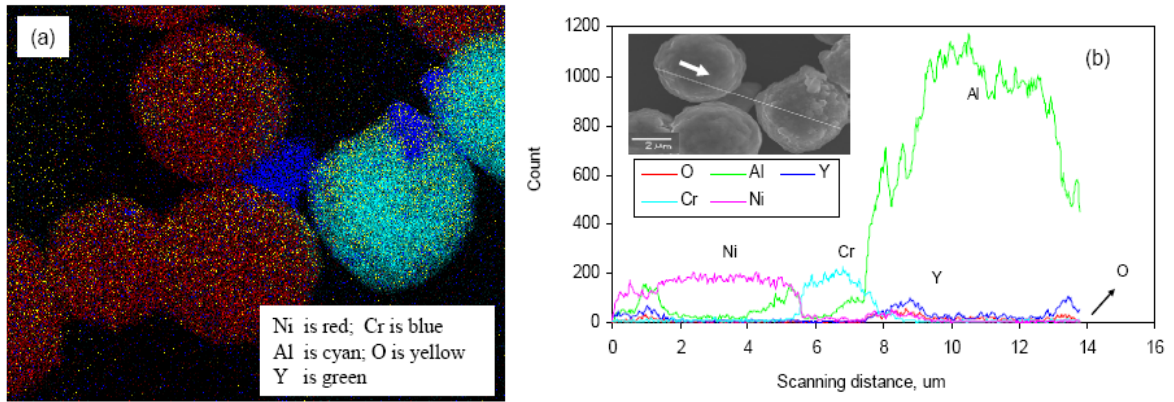


Figure 6 SEM EDX mapping micrographs and EDX line scanning profile of MCB processed powder sample A1, (a). Mapping of sample A1; (b) line scanning of across particles

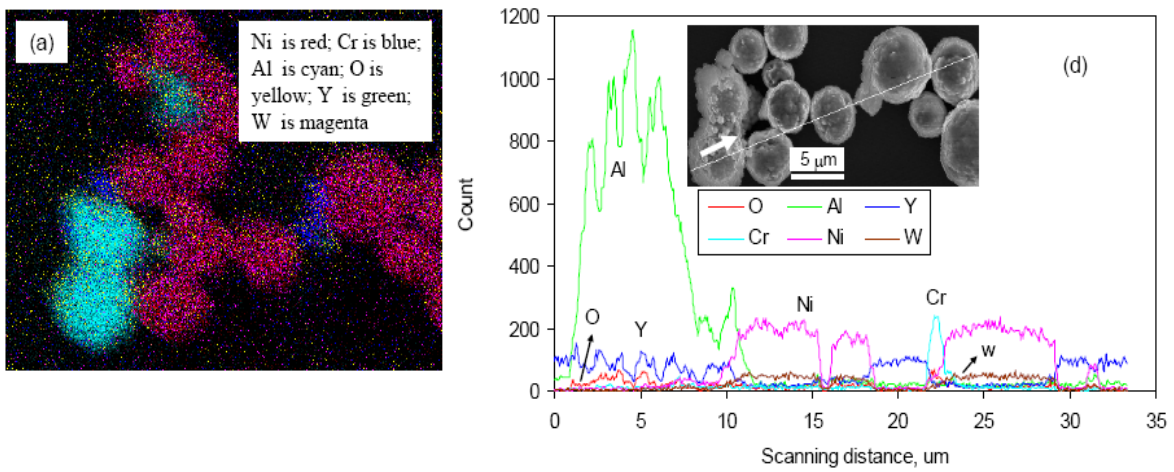


Figure 7 SEM EDX mapping micrographs and EDX line scanning profile of MCB processed powder sample A2, (a). Mapping of sample A2; (b) line scanning of across particles

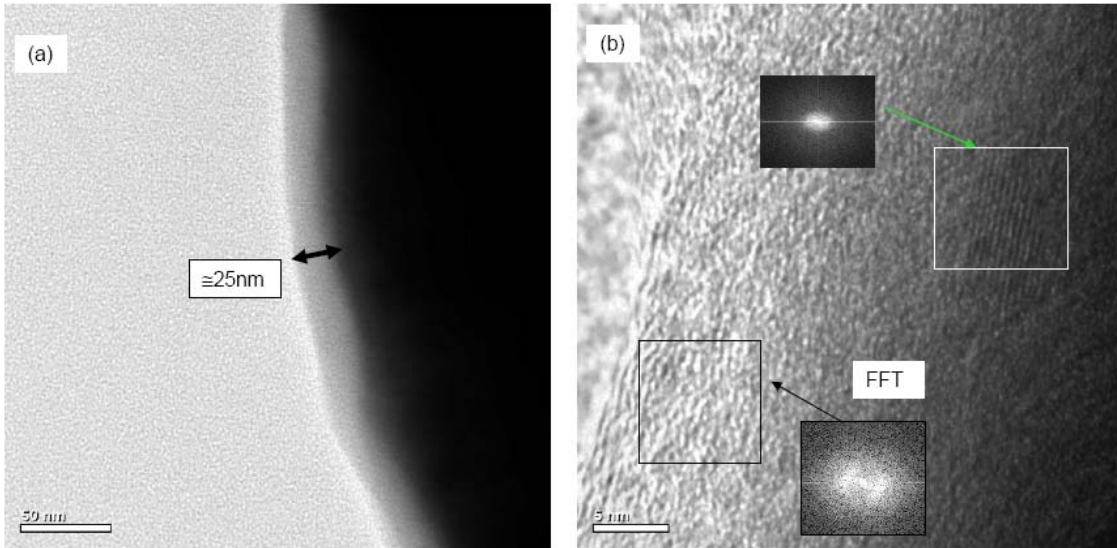


Figure 8 TEM BF and HRTEM images of the MCB processed powder sample A1
 (a) BF image, (b) HRTEM image of (a)

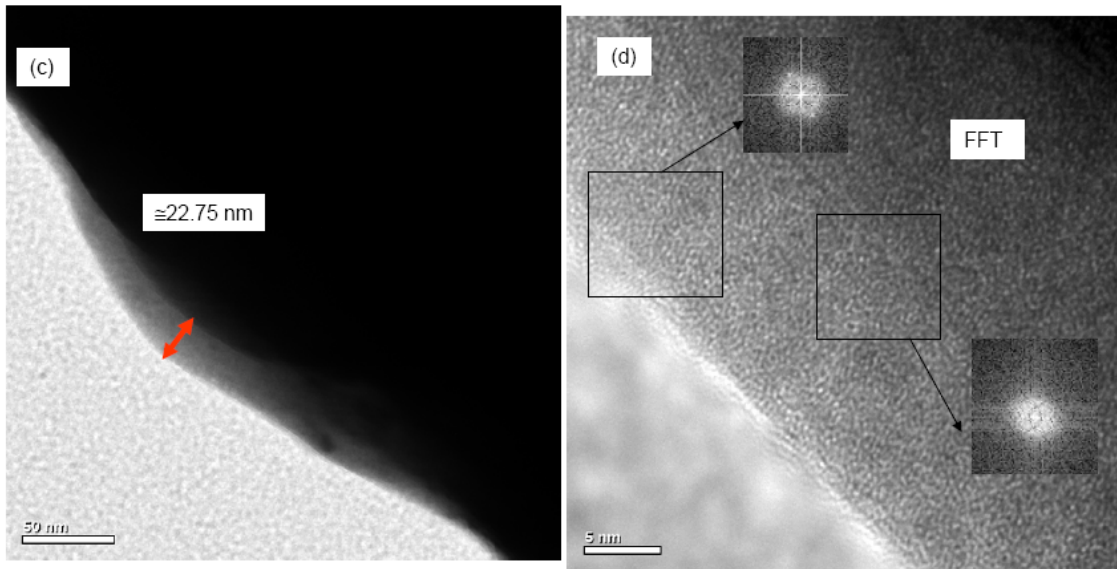


Figure 9 TEM BF and HRTEM images of the MCB processed powder sample A2
 (a) BF image, (b) HRTEM image of (a)

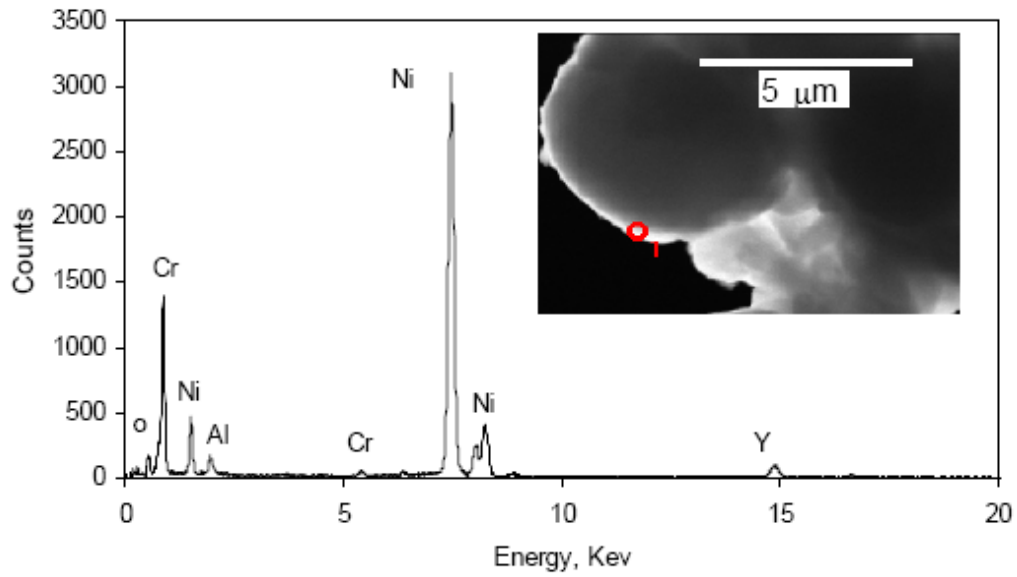


Figure 10 STEM image and EDX of sample A1

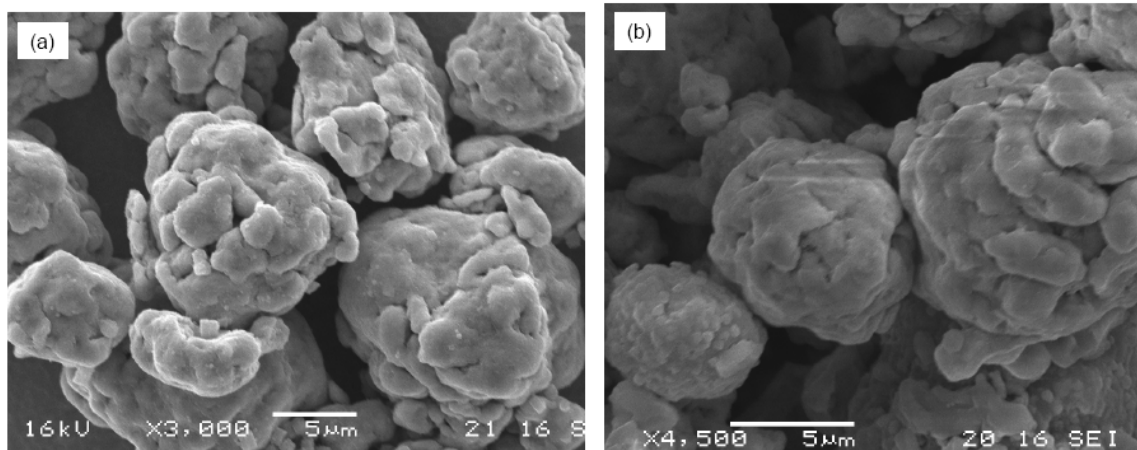


Figure 11 SEM micrographs of MCB processed powder sample B1 and B2
(a) Sample B1, (b) sample B2

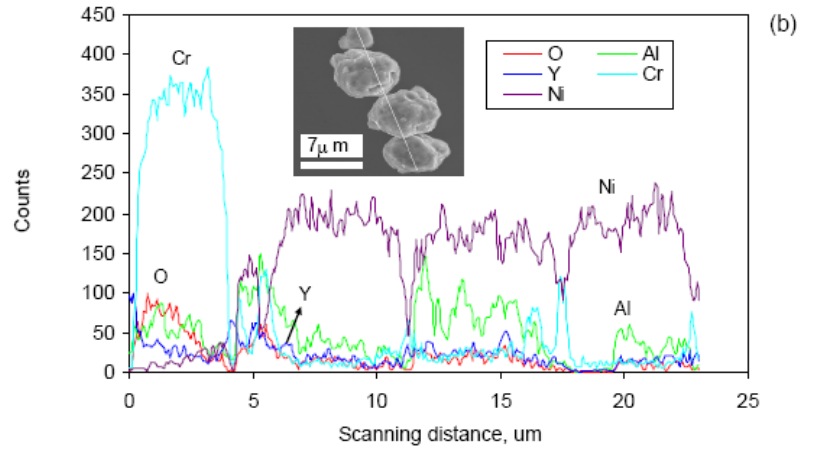
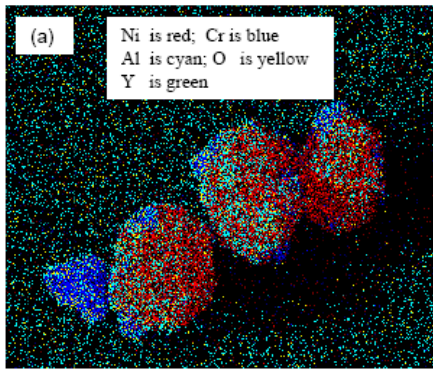


Figure 12 SEM EDX mapping micrographs and EDX line scanning profile of MCB processed powder sample B1
 (a) Mapping of sample B1, (b) line scanning of across particles

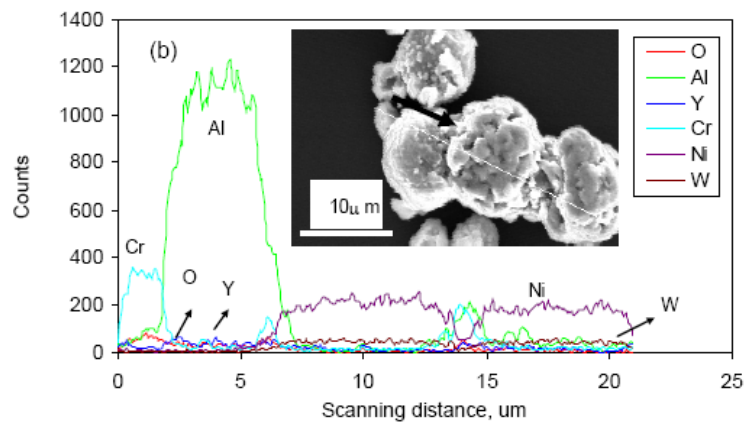
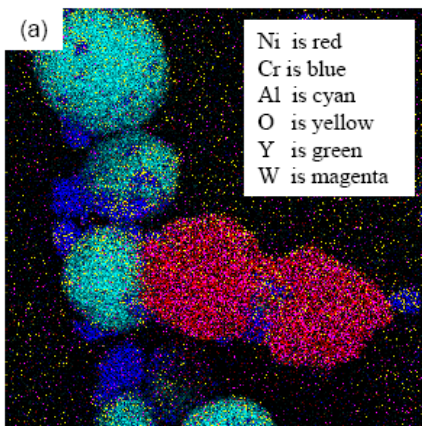


Figure 13 SEM EDX mapping micrographs and EDX line scanning profile of MCB processed powder sample B2
 (a) Mapping of sample B2, (b) line scanning of across particles

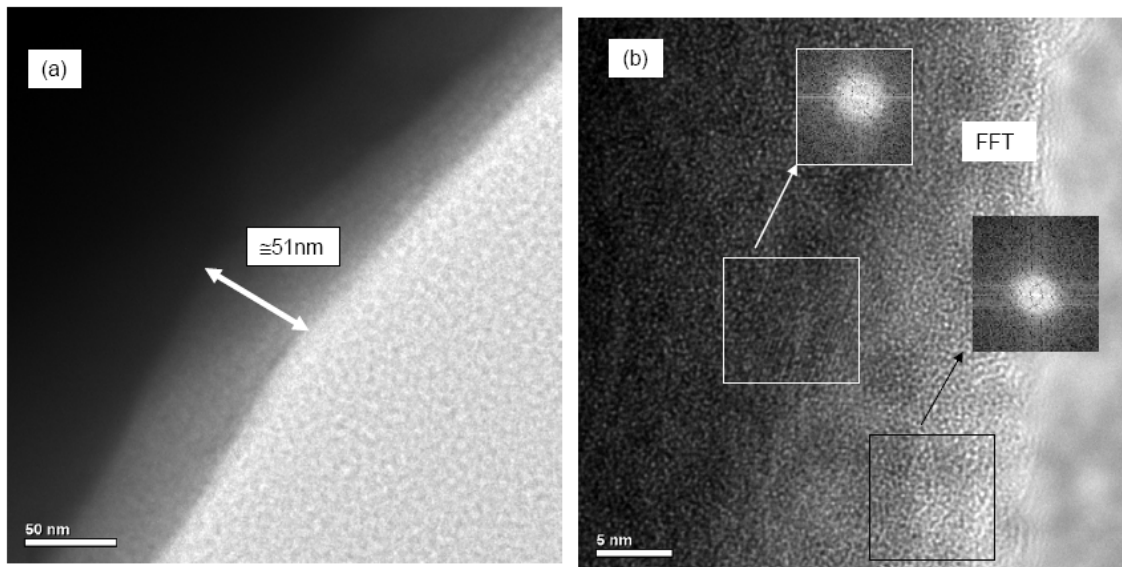


Figure 14 TEM BF and HRTEM images of the MCB processed powder sample B1
 (a) BF image, (b) HRTEM image of (a)

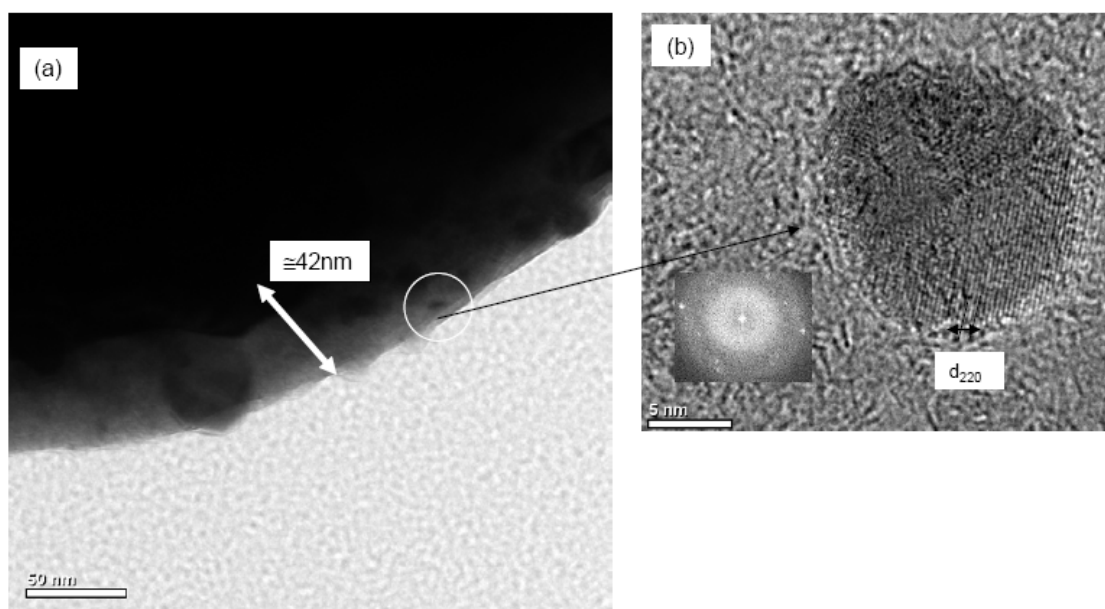


Figure 15 TEM BF and HRTEM images of the MCB processed powder sample B2
 (a) BF image, (b) HRTEM image of (a)

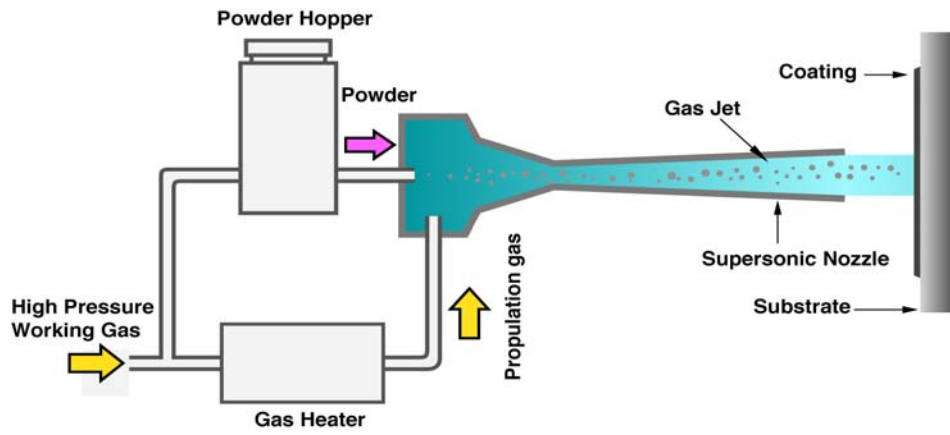


Figure 16 Cold spray schematic

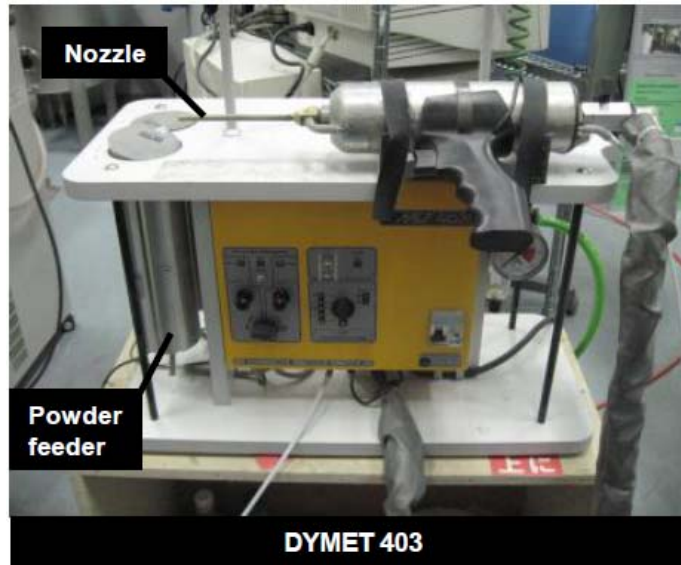


Figure 17 Dymet LP cold spray system

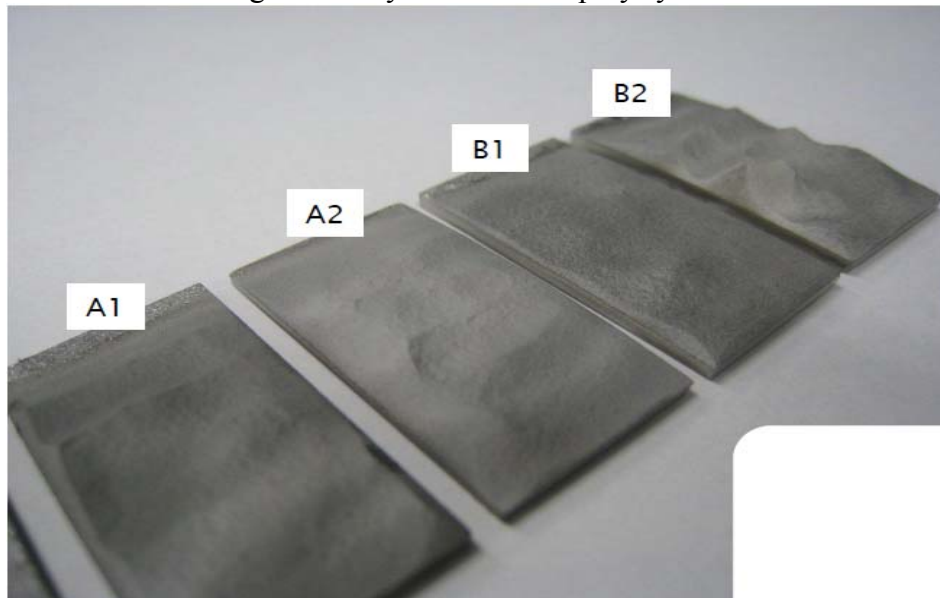


Figure 18 As-sprayed ODS coatings, four passes, 10 mm-off by hands

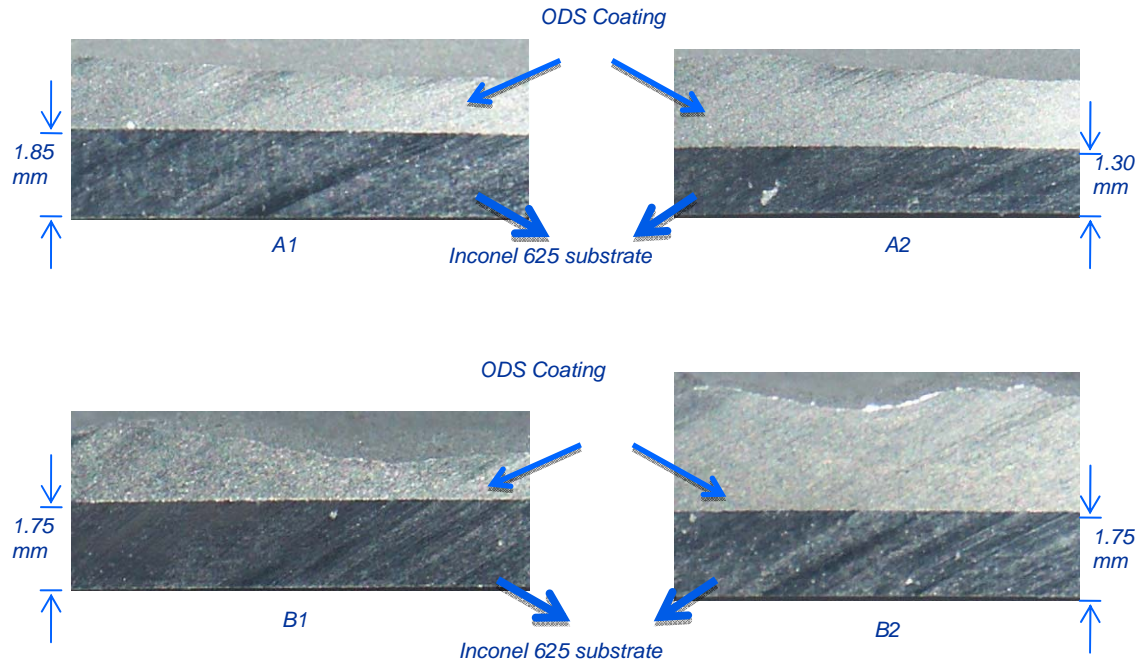


Figure 19 Cross-sectional view of the ODS coatings

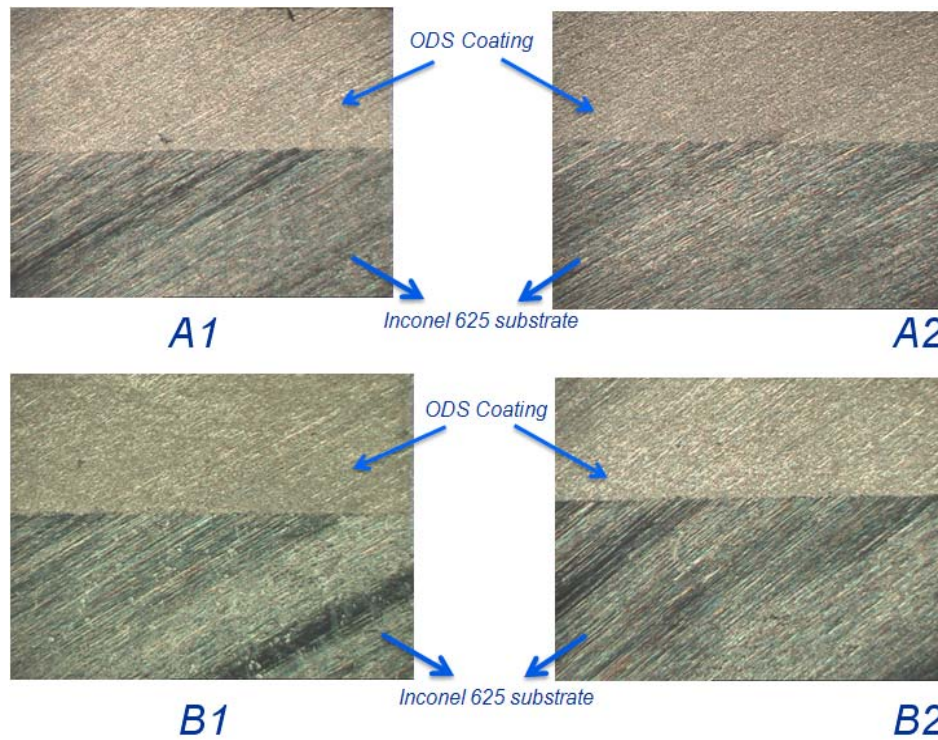


Figure 20 Interfacial region of the ODS coatings

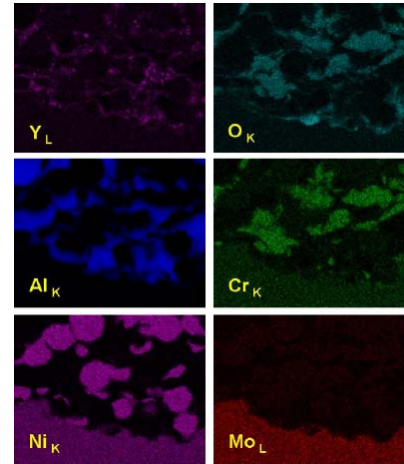
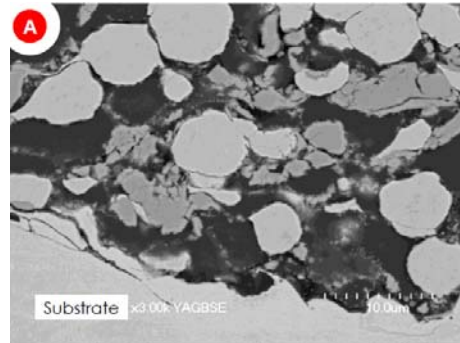
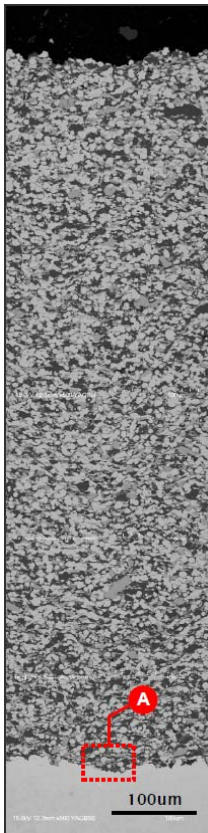


Figure 21 A1 coating and EDX map

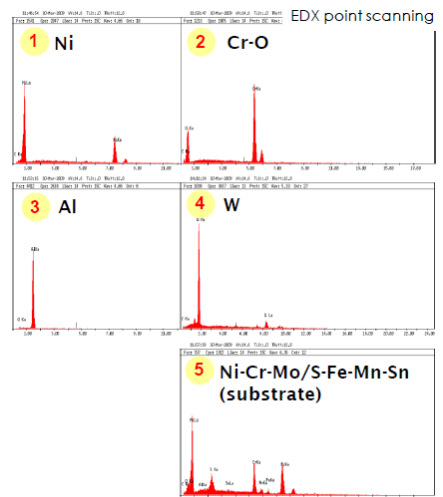
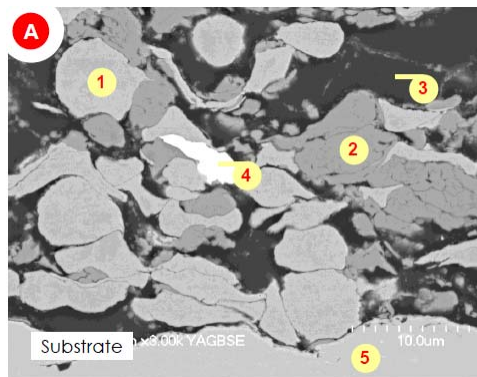
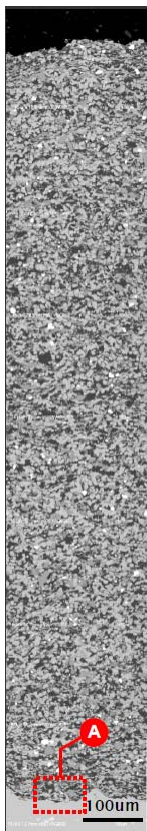


Figure 22 A2 coating and EDX plots

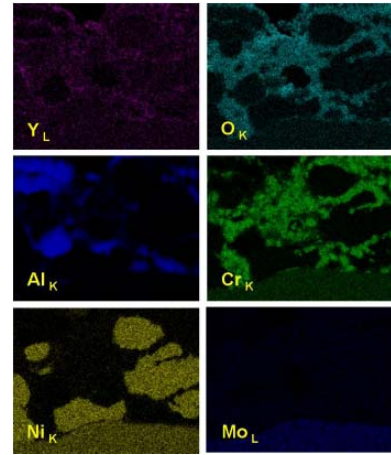
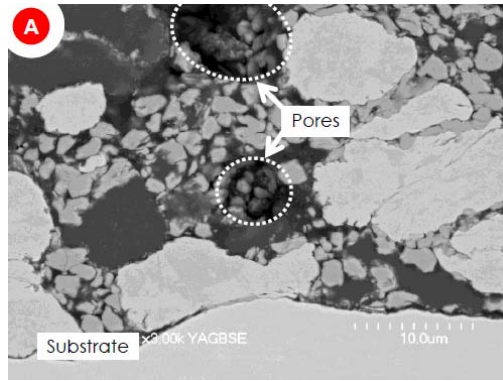
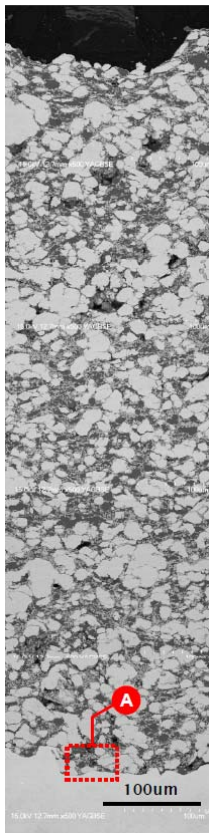


Figure 23 B1 coating and EDX map

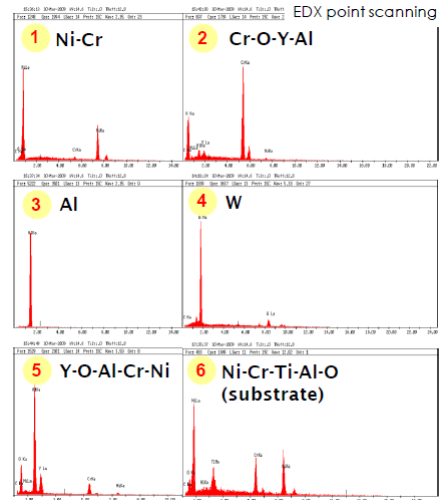
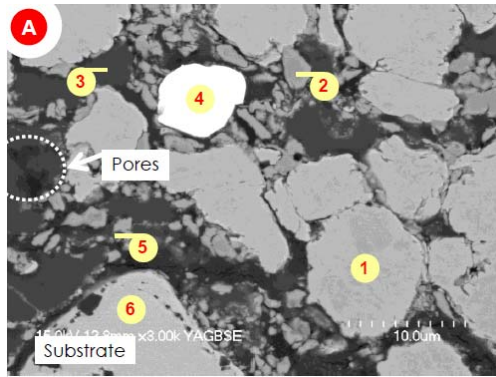
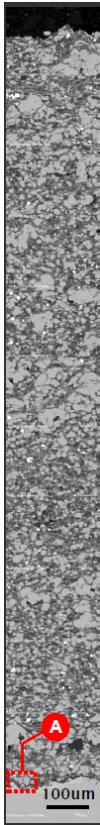


Figure 24 B2 coating and EDX plots